Antibiotic discovery with artificial intelligence for the treatment of Acinetobacter baumannii infections

Younes Smani (✉ ysma@upo.es)

 Andalusian Center of Developmental Biology, CSIC, University of Pablo de Olavide - Seville (Spain)

Yassir Boulaamane

 Laboratory of Innovative Technologies, National School of Applied Sciences of Tangier

Irene Molina Panadero

 Centro Andaluz de Biología del Desarrollo

Abdelkrim Hmadcha

 CABIMER   https://orcid.org/0000-0002-4105-3702

Celia Atalaya Rey

 Centro Andaluz de Biología del Desarrollo

Soukayna Baammi

 African Genome Centre (AGC)

Achraf El Allali

 College of Computing   https://orcid.org/0000-0002-4561-2161

Amal Maurady

 Laboratory of Innovative Technologies, National School of Applied Sciences of Tangier

---

Abstract

The global challenges presented by multidrug-resistant Acinetobacter baumannii infections have stimulated the development of new treatment strategies. We reported that OmpW is a potential therapeutic target in Acinetobacter baumannii. Here, a library of 11,648 natural compounds was subjected to a primary screening using QSAR models generated from a ChEMBL dataset with >7,000 compounds with their reported MIC values against A. baumannii followed by a structure-based virtual screening against OmpW. In silico ADME evaluation was conducted to assess the drug-likeness of these compounds. The ten highest-ranking compounds were found to bind with an energy score ranging from -7.8 to -7.0 kcal/mol where most of them belonged to curcuminoids. To validate these findings, one lead compound exhibiting promising binding stability as well as favourable pharmacokinetics properties, namely demethoxycurcumin was tested against a panel of A. baumannii strains to determine its antibacterial activity using microdilution and time-kill curve assays. To validate whether the compound binds to the selected target, an OmpW-deficient mutant was also studied and compared to the wild-type. Our results demonstrate that demethoxycurcumin in monotherapy and in combination with colistin is active against all A. baumannii strains. Moreover, an increased bacterial growth was observed in the OmpW-deficient mutant suggesting the importance of OmpW for the compound to exhibit its antibacterial activity. Finally, the compound was found to significantly reduce the interaction of A. baumannii with host cells suggesting its anti-virulence properties. Collectively, this study demonstrates artificial intelligence as a promising strategy for the discovery of curcuminoids as antimicrobial agents for combating A. baumannii infections.

INTRODUCTION

Antimicrobial resistance (AMR) in Gram-negative bacteria (GNB) has become a serious problem in recent years, with potentially devastating impacts on the economy and human life [1]. The need for more effective and safer antimicrobial compounds has become increasingly urgent in the post-antibiotic era [1]. *A. baumannii*, one of the six superbug ESKAPE pathogens, is a global priority pathogen for the development of effective antimicrobial therapies, due to rapid changes in the genetic constitution of *A. baumannii* and the plasticity to acquire different resistance mechanisms [2–4]. The scarce development of efficient antibiotics against this microorganism has sparked renewed scientific interest in finding effective antimicrobial agents capable of killing, inhibiting growth, or inhibiting the activity of essential virulence factors of *A. baumannii* [5].

The extensive functions of outer membrane proteins (OMPs) in GNB have led to their identification as potential drug targets [6]. Among the OMPs, outer membrane protein W (OmpW) is a porin playing a pivotal role in the uptake of nutritional substances such as iron [7]. Several studies have highlighted the relevance of OmpW as a potential drug target in GNB. For instance, researchers investigated how *A. baumannii* adapts to low oxygen conditions during infection. They found that OmpW was downregulated in hypoxic conditions. To understand its role as a virulence factor, they studied the effects of OmpW loss in *A. baumannii*. They discovered that the absence of OmpW reduced *in vitro* the bacterium's ability to

adhere to and invade host cells, to cause cell death and to form biofilm without affecting its growth, and *in vivo* the pathogenicity of *A. baumannii* [8]. Similarly, *V. cholerae* mutant strains lacking OmpW showed reduced colonization in the mouse intestine compared to strains expressing OmpW [9]. The collective evidence from these studies strongly suggests that OmpW plays a crucial role in bacterial pathogenesis and could be a promising target for the development of drugs aimed at combating GNB infections.

Natural products have long been a subject of great interest in the development of novel antimicrobial drugs [10]. These products, derived from plants, animals, and microorganisms, have been used for centuries by various traditional medicine systems to treat infections [11].

Chemical libraries enable comprehensive virtual drug screening by offering a diverse range of compounds. Large databases enhance the integration of advanced methods like machine learning and artificial intelligence for accurate prediction of drug properties. For example, MIT researchers used artificial intelligence to identify a potent new antibiotic known as halicin. This compound demonstrates efficacy against a wide range of bacteria, including some that exhibit resistance to all known antibiotics. Furthermore, halicin displayed no significant side effects in mice, prompting researchers to plan further development and clinical trials [12]. Recently discovered by researchers at the University of Toronto in 2021, abaucin exhibits promising efficacy against the lethal superbug *A. baumannii*. Although still in early development, it holds significant potential in the treatment of drug-resistant infections [13].

Thus, the objective of the present study was to screen a large library of natural products with potential activity against *A. baumannii* using "*in silico*" and "*in vitro*" assays. The screening focused on compounds targeting the function of OmpW. A library of 11,648 natural compounds was retrieved from Ambinter chemical library, and an *in-silico* approach combining data-driven and molecular modeling methods for drug discovery was employed. Artificial based quantitative-structure activity relationship (QSAR) models were developed to predict the bioactivity of the natural products against *A. baumannii*. The retained compounds were subsequently subjected to molecular docking screens and ADME evaluation to assess their pharmacological and pharmacokinetic profiles. The best compounds, which exhibited a strong affinity for OmpW along with favourable pharmacokinetic properties were further evaluated through molecular dynamics simulations. Finally, a lead candidate was subjected to *in vitro* testing to assess its potential for inhibiting *A. baumannii* growth.

RESULTS

QSAR screening

The quality of the developed machine learning and deep learning based QSAR classification models was assessed using the receiver operating characteristic (ROC) curve, which plots the true positive rate against the false positive rate [14]. Notably, all the classification models achieved an area under the curve (AUC) values higher than 0.80 as shown in Figure 1. The performance of the QSAR models was further evaluated using various performance metrics, as presented in Table 1. The convolutional neural network

(CNN) model performed exceptionally well on the testing and validation sets and was selected to predict the activity of Ambinter natural compounds library. At this stage, 1,193 compounds out of 6,151 were predicted as active against A. *baumannii* and were selected for the structure-based virtual screening study.

Docking screens of natural products

The quality assessment of the AlphaFold model of OmpW, according to Ramachandran plot, shows 92.2% of residues of are in most favourable regions, 7.2% in allowed regions, 0.6% in generously disallowed regions and 0.0% in disallowed regions. Validation of the OmpW structure using PROSA-web shows Z-score value of −4.95 which is within the range of scores typically found for native proteins of similar size (Figure 2A and 2B). The predicted active compounds were subjected to molecular docking screens, and their binding affinities were ranked accordingly. Specifically, we observed that the highest-ranking compounds exhibit binding scores ranging from -7.0 to -7.8 kcal/mol and belong to curcuminoids as shown in Figure 2C. The amino acids involved in the ligand binding are presented in Table 2.

Docking poses of the highest-ranking compounds are displayed in Figure 3. In brief, the structural analysis of the docked compounds reveals consistent hydrogen bond formation between the hydroxyl (-OH) group of the phenyl ring in curcuminoids and the amino acid residue GLN-23. Furthermore, we detected additional hydrogen bond interactions implicating key residues, namely ASN-104, THR-109, and LYS-195, situated within the periplasmic site of OmpW. Additionally, our analysis reveals multiple instances of hydrophobic interactions, with notable involvement of amino acid residues PHE-59, HIS-101, ASN-144, and GLN-146.

ADME evaluation

A significant proportion, approximately 40%, of drug candidates fail during clinical trials primarily due to inadequate ADME properties [15]. *In silico* ADME prediction offers a rapid method to assess the drug-likeness of a compound by calculating its physicochemical properties. This approach substantially reduces the time and resources required during the overall drug development process. In this study, SwissADME (http://www.swissadme.ch/) was employed to compute various pharmacokinetic properties of the highest-scoring compounds to evaluate their drug-likeness and suitability for further experimental studies [16]. ADME properties for the selected compounds are shown in Table 3. The results reveal that all the compounds possess a good lipophilicity in accordance with Lipinski's rule of five, moreover water solubility values were found to be in the recommended range for most drugs. Intestinal absorption was found to be high in all the compounds. Out of the top ten compounds tested for blood-brain barrier (BBB) permeability, only five were found to be unable to penetrate the BBB. This is a crucial finding, as antibacterial compounds should not exert their effects on the central nervous system (CNS). None of the compounds were found to act as a P-gp substrate, thus their bioavailability is not impacted by this

protein. Finally, PAINS test has revealed four compounds presenting one alert in their structure due to the presence of the catechol group which can result in non-specific binding with various target proteins.

Molecular dynamics simulations and binding free energy

In the molecular docking study, the protein structure was treated as rigid. To gain deeper insights into the protein-ligand interactions, molecular dynamics simulations were performed on the docked complexes in a water environment for 100 ns. The root-mean square deviation (RMSD) was measured relative to the OmpW structure bound to the selected candidates. Figure 4A illustrates the protein RMSD values for the top four complexes, showing a consistently stable RMSD of 0.3 nm during most of the simulation, except for Amb22174074, which displayed higher fluctuations exceeding 0.3 nm in the last 20 ns. The analysis of the ligand RMSD showed values between 0.1 and 0.25 nm for most ligands, suggesting minor conformational changes during the simulation. However, the ligand Amb8399162 deviated from this trend, with an RMSD of 0.35 nm, suggesting a more significant conformational change (Figure 4B). In Figure 4C, the graph illustrates the variations observed in each amino acid. Notably, the N-terminal region exhibited the highest fluctuations, which is a common characteristic. For all other residues, minor fluctuations of approximately 0.1 nm were observed, except for Amb8399162, which displayed fluctuations higher than 0.2 nm in certain regions of the periplasm. Finally, hydrogen bonds within a proximity of 0.35 nm were documented. Figure 4D depicts the hydrogen bonds observed at 100 ns, with Amb2698241 forming four hydrogen bonds, highlighting its stable and consistent binding to the protein. The average free binding energy of the selected complexes was determined using the g_mmpbsa package [17].

The binding energy was computed by combining the scores of Van der Waals energy, electrostatic energy, polar solvation, and SASA energy as presented in Table 4. The highest binding energy was observed in Amb2698241 (-45.23 kJ/mol) suggesting a strong binding to the target protein.

Antibacterial activity

The best compound exhibiting the lowest docking score as well as favourable ADME properties was demethoxycurcumin (Amb2698241). The MIC was then assessed using microdilution assays against different reference *A. baumannii* ATCC 17978 strain, its isogenic mutant deficient in OmpW, and colistin-resistant *A. baumannii* clinical isolates. Demethoxycurcumin inhibited bacterial growth at a concentration of 64 µg/mL for all the studied strains (Table 4).

Colistin potentiation is critical for safeguarding this last resort antibiotic as it is often our only treatment option against highly resistant Gram-negative pathogens. We examined whether demethoxycurcumin can sensitize colistin-resistant clinical strain CR17. Chequerboard assay showed that demethoxycurcumin at >=1 mg/L demonstrated synergy with colistin against CR17 strain. Demethoxycurcumin >= 8 mg/L in combination with colistin increased the activity of colistin against CR17 strain, with a fractional inhibitory

concentration index (FICI) of <0.2 (Figure 5A). In addition, the combination between 16 mg/L demethoxycurcumin and 1 mg/L colistin exhibited a synergistic effect during 2 and 4 h, reducing significantly the bacterial growth compared with colistin demethoxycurcumin alone (Figure 5B).

Using bacterial growth assays, we examined the antibacterial activity of demethoxycurcumin against ATCC 17978 and ΔOmpW strains. Figure 5C reveals that *A. baumannii* ATCC 17978exhibits rapid growth, reaching 0.5 OD within the first 4 h. However, a noticeable disparity in growth is observed between the control sample and the samples treated with demethoxycurcumin, particularly at higher compound concentrations (2xMIC and 4xMIC). A similar trend of growth inhibition is observed in the ΔOmpW strain, although it demonstrates a higher OD value compared to *A. baumannii* ATCC 17978 in presence of demethoxycurcumin treatment.This disparity in growth can be attributed to the resistance of the mutant strain to the compound, as the absence of OmpW may hinder the compound's ability to exert its effect, as indicated by the findings of the molecular docking study.

In addition, and to evaluate the effect of demethoxycurcuminon *A. baumannii* interaction with host cells, we studied the adherence of ATCC 17978 and ΔOmpW strains to HeLa cells for 2 h in the presence of demethoxycurcumin. Treatment with demethoxycurcumin at 1xMIC reduced the adherence of ATCC 17978 and ΔOmpW strains to HeLa cells by 36% and 16%, respectively (Figure 5D).

DISCUSSION

In this study, we present a multi-stage approach for screening bioactive compounds from extensive databases. This approach combines data-driven QSAR models and structure-based virtual screening methods for drug discovery. Our classification models demonstrated strong performance in distinguishing between active and inactive compounds, achieving AUC values ranging from 0.85 to 0.96 for the testing set and 0.84 to 0.96 for the validation set. The results of molecular docking indicated binding affinities spanning from − 5.4 to -7.8 kcal/mol. Notably, the top-scoring compounds belong to the curcuminoid chemical class, recognized for their antibacterial activities [18, 19].

Analysis of molecular interactions revealed a consistent hydrogen bond formation with GLN-23 in most of the compounds under study. Additional hydrophobic interactions involved the amino acids: PHE-59, HIS-101, ASN-144, and GLN-146. Molecular dynamics analysis of the first four complexes displayed remarkable stability throughout the simulation, except for the tricyclic compound Amb22174074, which exhibited some deviations, leading to an RMSD of 0.3 nm. This observation could be attributed to the inherent limited flexibility of this compound, prompting conformational changes in the protein.

Furthermore, our investigation identified van der Waals energy as the primary contributor to the stability of the complexes, as determined by the MMPBSA method. To validate our *in-silico* results, we assessed a lead candidate, demethoxycurcumin, for its *in vitro* activity in monotherapy and in combination with colistin against an extensive range of *A. baumannii* strains, including colistin-resistant strains. This lead candidate presents an antibacterial activity as showed by microdilution and time-kill curve assays. Notably, a reduction in compound activity against OmpW-deficient mutant has been observed in the time-

kill curve assay. Li et al. showed that demethoxucurcumin present antibacterial activity in monotherapy and combination with gentamicin against another pathogen, the methicillin-resistance *Staphylococcus aureus* [20]

Our findings suggest the crucial role of the OmpW in facilitating the compound's activity. Previous studies reported the binding of colistin and tamoxifen metabolites to OmpW [21, 22].

Bacterial adhesion to and invasion into host cells are important steps in causing *A. baumannii* infection [23]. It is well-known that OmpW plays a key role in host-pathogen interactions. Deletion of OmpW reduced *A. baumannii*'s adherence and invasion into host cells, as well as its cytotoxicity [8]. Similarly, in the absence of OprG, which is homologous to OmpW in *P. aeruginosa*, this pathogen was significantly less cytotoxic against human bronchial epithelial cells [24]. OmpW is essential for *A. baumannii* to disseminate between organs and to cause the death of mice, as observed for other pathogens such as *Vibrio cholerae* [25]. Motley et al. reported an increase in OmpW expression during *E. coli* infection in a murine granulomatous pouch model [26], and OmpW has been shown to protect *E. coli* against host responses, conferring resistance to complement-mediated killing and phagocytosis [27, 28]. All these previous studies indicated that OmpW could be a potential drug target in GNB to develop new treatments. However, no data have been reported on the effect of natural products on host-*A. baumannii* interactions. To our knowledge, this study provides the first evidence for the effect of demethoxycurcumin in reducing *A. baumannii*'s adherence to host cells. Moreover, this effect is consistent with time-kill curve data. Further studies are needed, such as animal infection models, to validate the potential use of demethoxycurcumin as monotherapy and in combination with antibiotics used in clinical settings.

In summary, this study demonstrated a multi-step computational and experimental approach to identify natural products as potential therapeutics targeting the OmpW protein of *A. baumannii*. Demethoxycurcumin was validated as an active lead compound both *in vitro* and in reducing bacterial interaction with host cells. Further investigations are necessary, such as testing in animal models of infection, to validate the therapeutic potential of targeting OmpW by demethoxycurcumin and related natural products.

MATERIALS AND METHODS

QSAR modeling

A bioactivity dataset from the ChEMBL database, which comprised the chemical structures of 11,014 compounds along with their reported MIC values against *A. baumannii* was acquired [29]. To ensure the reliability of the data, the dataset by only keeping those with MIC values of the same unit (mg/L) was carefully curated. For duplicate compounds with multiple reported activities, a mean value was calculated and only one entry was kept in the study using the Pandas library in Python [30]. The processed dataset consisted of 3,196 compounds. To classify the compounds, molecules with reported MIC values < 32 were labelled as active while molecules with MIC > 64 were labelled as inactive. This resulted in 1,310

active compounds and 816 inactive compounds. For further analysis, the RDKit cheminformatics suite to generate 2,048 bits of molecular descriptors using Morgan fingerprints [31]. These descriptors were derived from the compounds' SMILES representation and were based on the widely used extended-connectivity fingerprints (ECFP4) [32]. To train and evaluate our QSAR models, the datasets were partitioned using a 3:1:1 ratio for train/test/validation, as shown in Fig. 6.

To evaluate the performance of the machine learning and deep learning models, several statistical metrics described previously were employed [33]. These metrics encompassed the calculation of sensitivity (Eq. 1), specificity (Eq. 2), predictive positive value (Eq. 3), predictive negative value (Eq. 4), accuracy (Eq. 5), and Matthews' correlation coefficient (Eq. 6). The equations used for computing these metrics were as follows:

$$SE = \frac{TP}{(TP+FN)} \text{ (1)} \quad SP = \frac{TN}{(FP+TN)} \text{ (2)}$$

$$Q+ = \frac{TP}{(TP+FP)} \text{ (3)} \quad Q- = \frac{TN}{(TN+FN)} \text{ (4)}$$

$$ACC = \frac{(TP+TN)}{(P+N)} \text{ (5)} \quad MCC = \frac{(TP \times TN)-(FP \times FN)}{\sqrt{(TP+FP)*(TP+FN)*(TN+FP)*(TN+FN)}} \text{ (6)}$$

Protein structure preparation

As the full three-dimensional structure of none of the proteins was available in the Protein Data Bank (PDB), the homology model of OmpW was downloaded from AlphaFold (Uniprot ID: A0A335FU53) [34]. The online server GalaxyRefine (https://galaxy.seoklab.org/cgi-bin/submit.cgi?type=REFINE) was used to refine and improve the quality of three-dimensional protein models [35]. The platform employs a multi-step approach that involves side chain rebuilding, side-chain repacking, and molecular dynamics simulation to achieve overall structure relaxation. Subsequently, PROCHECK algorithm was employed through SAVES webserver (https://saves.mbi.ucla.edu/) [36] to generate Ramachandran plots, while ProSA-web was used to assess model accuracy and statistical significance using a knowledge-based potential [37].

Binding site detection

The plausible binding pockets for the selected OmpW protein structure was predicted using PrankWeb ligand binding site prediction webserver (https://prankweb.cz/) [38, 39]. Figure S1 depicts the 3D structure of OmpW with their predicted binding pockets shown as residues with different colours. The predicted binding pockets scores, grid coordinates and residue IDs are shown in Table S1.

Structure-based virtual screening

The natural compounds were retrieved from Ambinter natural compounds library (https://www.ambinter.com/). 11,648 compounds were evaluated for their druglikeness by computing their physicochemical properties such as molecular weight, LogP, number of hydrogen bond

donors/acceptors and the number of rotatable bonds. According to Lipinski's rule of five only 6,151 compounds were retained for further analysis [40]. Structure-based virtual screening was performed using AutoDock Vina with a Perl script to automate the molecular docking process as published in our previous study [41, 42]. The 3D structure of OmpW were optimized using AutoDockTools by adding polar hydrogens and computing Kollman charges [43]. The grid box was centred around the coordinates provided by PrankWeb for the best-scoring pockets. The pocket (2) located near the periplasmic of the β-barrel structure was selected for molecular docking as mentioned in the literature [44].

Molecular dynamics simulations and binding free energy calculation

Molecular dynamics simulations were performed using GROMACS (version 2019.3) [45] to evaluate the stability of selected candidates in complex with OmpW. The CHARMM36 force field generated the protein topology file, while the CGENFF server assigned parameters to ligands [46]. TIP3P water model solvated the protein-ligand systems in a cubic box, with Na + and Cl − ions added for charge neutrality. To optimize the energy, the steepest descent technique was employed, setting Fmax not to exceed 1000 kJ/mol/nm. Subsequently, two consecutive 1 ns simulations using canonical NVT, and isobaric NPT ensembles were performed to equilibrate the systems at 300 Kelvin and 1 bar pressure. All simulations were conducted under periodic boundary conditions (PBC), and long-range electrostatic interactions were handled using the particle mesh Ewald method [47]. For data collection, 100 ns molecular dynamics simulations were conducted [48, 49]. To analyse the dynamic behaviour of the selected complexes, various geometric properties such as root-mean-square deviation (RMSD), root-mean-square fluctuation (RMSF), and hydrogen bonds were calculated using GROMACS package.

The binding free energies of the screened complexes were calculated using the Molecular Mechanics Poisson−Boltzmann Surface Area (MM-PBSA) method [50]. The binding free energy ($\Delta E_{binding}$) is determined using the following equations:

$$\Delta E_{binding} = E_{complex} - \left(E_{inhibitor} + E_{OmpW} \right)$$

1

Equation (1) is the total MMPBSA energy of the protein-ligand complex, where E_{OmpW} and $E_{inhibitor}$ are the isolated proteins and ligands' total free energies in solution, respectively.

$$\Delta G_{binding} = \Delta G_{vdW} + \Delta G_{elec} + \Delta G_{solv} + \Delta G_{sasa}$$

2

Equation (2) defines the generalized MMPBSA as the sum of four energies: electrostatic (ΔG_{elec}), van der Waals (ΔG_{vdw}), polar (ΔG_{solv}), and SASA (ΔG_{sasa}).

Antibacterial activity assays

Microdilution assay. The MIC of demethoxycurcumin was determined against ATCC 17978 strain and isogenic mutant deficient in OmpW and seven colistin-resistant *A. baumannii* clinical strains 24 clinical strains in two independent experiments using the broth microdilution method, in accordance with the standard guidelines of the European Committee on Antimicrobial Susceptibility Testing (EUCAST) [51]. A $5x10^5$ CFU/mL inoculum of each strain was cultured in Luria Bertani (LB) and added to U bottom microtiter plates (Deltlab, Spain) containing demethoxycurcumin. The plates were incubated for 18 h at 37 ºC.

Bacterial growth curve assay. To determine the antibacterial activity, bacterial growth curves of the ATCC 17978 strain and its isogenic deficient in OmpW (ΔOmpW), and CR17 strain were performed in duplicate in 96-well plate (Deltlab, Spain). An initial inoculum of $5x10^5$ cfu/mL was prepared in LB in the presence of 1xMIC, 2xMIC, and 4xMIC of demethoxycurcumin. A drug-free broth was evaluated in parallel as a control. Plates were incubated at 37ºC with shaking, and bacterial growth was monitored during 24 h using a microtiter plate reader (Tecan Spark, Austria).

Checkerboard assay. The assay was performed on a 96-well plate as previously described [52]. Colistin was 2-fold serially diluted along the x axis, whereas demethoxycurcumin was 2-fold serially diluted along the y axis to create a matrix, where each well consists of a combination of both agents at different concentrations. Bacterial cultures grown overnight were then diluted in saline to 0.5 McFarland turbidity, followed by 1:50 further dilution LB and inoculation on each well to achieve a final concentration of approximately $5.5x10^5$ cfu/mL. The 96-well plates were then incubated at 37°C for 18 h and examined for visible turbidity. The fractional inhibitory concentration (FIC) of the colistin was calculated by dividing the MIC of colistin in the presence of demethoxycurcumin by the MIC of colistin alone. Similarly, the FIC of demethoxycurcumin was calculated by dividing the MIC of demethoxycurcumin in the presence of colistin by the MIC of rafoxanide alone. The FIC index was the summation of both FIC values. FIC index values of ≤ 0.5 were interpreted as synergistic.

Human cell culture

HeLa cells was grown in 24-well plates in DMEM supplemented with 10% heat-inactivated fetal bovine serum (FBS), vancomycin (50 mg/L), gentamicin (20 mg/L), amphotericin B (0.25 mg/L) (Invitrogen, Spain), and 1% HEPES in a humidified incubator with 5% CO_2 at 37°C. HeLa cells were routinely passaged every 3 or 4 days. Immediately before infection, HeLa cells were washed three times with prewarmed PBS and further incubated in DMEM without FBS and antibiotics [53].

Adhesion assay

HeLa cells were infected with $1×10^8$ CFU/ml of *A. baumannii* ATCC 17978 and ΔOmpW strains in absence and presence of 1xMIC of demethoxycurcumin at a multiplicity of infection (MOI) of 100 for 2 h with 5% CO_2 at 37°C. Subsequently, infected HeLa cells were washed five times with prewarmed PBS and lysed with 0.5% Triton X-100. Diluted lysates were plated onto LB agar (Merck, Spain) and incubated at

37°C for 24 h for enumeration of developed colonies and then the determination of the number of bacteria that attached to HeLa cells [8].

Statistical Analysis

Group data are presented as means ± standard errors of the means (SEM). The student t-test was used to determine differences between means using GraphPad Prism 9. A p-value < 0.05 was considered significant.

Declarations

DATA AVAILABILITY

The study's supporting data can be found in the main paper and its Supplementary Information. For any other data not included, interested parties can obtain them from the corresponding authors upon reasonable request. Additionally, the source data accompanying this paper are provided for reference.

AUTHORS CONTRIBUTION

Conceptualization, Y.B., A.M. and Y.S.; methodology, Y.B., I.M.P., A.H., S.B. and A.E.; formal analysis, Y.B. and Y.S.; writing—original draft preparation, Y.B. and Y.S.; writing-review and editing, Y.B. and Y.S.; and funding acquisition, Y.S. All authors have read and agreed to the published version of the manuscript.

COMPETING INTERESTS

The authors declare that they have no known competing financial interests or personal relationships that could have appeared to influence the work reported in this paper.

References

1. World Health Organization Global research agenda for antimicrobial resistance in human health Policy brief June 2023. https://cdn.who.int/media/docs/default-source/antimicrobial-resistance/amr-spc-npm/who-global-research-agenda-for-amr-in-human-health---policy-brief.pdf?sfvrsn=f86aa073_4&download=true

2. Tacconelli, E., et al. Discovery, research, and development of new antibiotics: the WHO priority list of antibiotic-resistant bacteria and tuberculosis. *Lancet Infect. Dis.***18**, 318-327 (2018).

3. Harding, C.M., Hennon, S.W., Feldman, M.F. Uncovering the mechanisms of *Acinetobacter baumannii*. *Nat. Rev. Microbiol.***16**, 91-102 (2018).

4. Theuretzbacher, U., Bush, K., Harbarth, S., Paul, M., Rex, J.H., Tacconelli, E., Thwaites, G.E. Critical analysis of antibacterial agents in clinical development. *Nat. Rev. Microbiol.***18**, 286-298 (2020).

5. Theuretzbacher, U., Outterson, K., Engel, A., Karlén, A. The global preclinical antibacterial pipeline. *Nat. Rev. Microbiol.***18**, 275-285 (2020).

6. Walker, S. S., Black, T. A. Are outer-membrane targets the solution for MDR Gram-negative bacteria?. *Drug discov. Today***26**, 2152-2158 (2021).

7. Schmitt, B. L., Leal, B. F., Leyser, M., de Barros, M. P., Trentin, D. S., Ferreira, C. A. S., de Oliveira, S. D. Increased OmpW and OmpA expression and higher virulence of *Acinetobacter baumannii* persister cells. BMC *Microbiology***23**, 1-8 (2023).

8. Gil-Marqués, M. L., Pachón, J., Smani, Y. iTRAQ-based quantitative proteomic analysis of *Acinetobacter baumannii* under hypoxia and normoxia reveals the role of OmpW as a virulence factor. *Microbiol. Spectr.***10**, e02328-21 (2022).

9. Nandi, B., Nandy, R. K., Sarkar, A., Ghose, A. C. Structural features, properties and regulation of the outer-membrane protein W (OmpW) of *Vibrio cholerae. Microbiology*, **151**, 2975-2986 (2005).

10. Chassagne, F., et al. A systematic review of plants with antibacterial activities: A taxonomic and phylogenetic perspective. *Front. Pharmacol.***11**, 2069 (2021).

11. Anand, U., Jacobo-Herrera, N., Altemimi, A., Lakhssassi, N. A comprehensive review on medicinal plants as antimicrobial therapeutics: potential avenues of biocompatible drug discovery. *Metabolites***9**, 258 (2019).

12. Stokes, J. M., Yang, K., Swanson, K., Jin, W., Cubillos-Ruiz, A., Donghia, N. M., ... & Collins, J. J. (2020). A deep learning approach to antibiotic discovery. Cell, 180(4), 688-702.

13. Liu, G., Catacutan, D. B., Rathod, K., Swanson, K., Jin, W., Mohammed, J. C., ... & Stokes, J. M. (2023). Deep learning-guided discovery of an antibiotic targeting Acinetobacter baumannii. Nature Chemical Biology, 1-9.

14. Zweig, M. H., Campbell, G. (1993). Receiver-operating characteristic (ROC) plots: a fundamental evaluation tool in clinical medicine. *Clin. Chem*. **3**, 561-577.

15. Gombar, V. K., Silver, I. S., Zhao, Z. Role of ADME characteristics in drug discovery and their *in silico* evaluation: in silico screening of chemicals for their metabolic stability. *Curr. Top. Med. Chem*. **3**, 1205-1225 (2003).

16. Daina, A., Michielin, O., Zoete, V. SwissADME: a free web tool to evaluate pharmacokinetics, drug-likeness and medicinal chemistry friendliness of small molecules. *Sci. Rep.***7**, 42717 (2017).

17. Kumari, R., Kumar, R., Open Source Drug Discovery Consortium, Lynn, A. g_mmpbsa A GROMACS tool for high-throughput MM-PBSA calculations. *J. Chem. Inf. Model***54**, 1951-1962 (2014).

18. Betts, J. W., Wareham, D. W. In vitro activity of curcumin in combination with epigallocatechin gallate (EGCG) versus multidrug-resistant *Acinetobacter baumannii. BMC Microbiol.* **14**, 1-5 (2014).

19. Othman, A. S., Shamekh, I. M., Abdalla, M., Eltayb, W. A., Ahmed, N. A. Molecular modeling study of micro and nanocurcumin with *in vitro* and *in vivo* antibacterial validation. *Sci. Rep.* **13**, 12224 (2023).

20. Li, Q.Q., Kang, O.K., Kwon., D.Y. Study on demethoxycurcumin as a promising approach to reverse methicillin-resistance of Staphylococcus aureus. *Int. J. Mol. Sci.* **22**, 3778 (2021).

21. Catel-Ferreira, M., et al. The outer membrane porin OmpW of *Acinetobacter baumannii* is involved in iron uptake and colistin binding. *FEBS Lett.* **590**, 224-231 (2016).

22. Vila-Domínguez, A., Molino Panadero, I., Pachón, J., Jiménez Mejías, M. E., Smani, Y. Identification of the outer membrane protein W (OmpW) as the potential target of tamoxifen metabolites in *Acinetobacter baumannii*. A two-day virtual conference on *Acinetobacter* research. AcinetoVibes (2022).

23. Smani, Y., Docobo-Pérez, F., López-Rojas, R., Domínguez-Herrera, J., Ibáñez-Martínez, J., Pachón, J. Platelet-activating factor receptor initiates contact of *Acinetobacter baumannii* expressing phosphorylcholine with host cells. *J. Biol. Chem.* **287**, 26901-26910 (2012).

24. McPhee, J. B., et al. The major outer membrane protein OprG of *Pseudomonas aeruginosa* contributes to cytotoxicity and forms an anaerobically regulated, cation-selective channel. *FEMS Microbiol. Lett.* **296**, 241-247 (2009).

25. Nandi B, Nandy RK, Sarkar A, Ghose AC. Structural features, properties and regulation of the outer-membrane protein W (OmpW) of Vibrio cholerae. *Microbiology* **151**, 2975-2986 (2005).

26. Motley, S. T., Morrow, B. J., Liu, X., Dodge, I. L., Vitiello, A., Ward, C. K., Shaw, K. J. Simultaneous analysis of host and pathogen interactions during an *in vivo* infection reveals local induction of host acute phase response proteins, a novel bacterial stress response, and evidence of a host-imposed metal ion limited environment. *Cell. Microbiol.* **6**, 849-865 (2004).

27. Li, W., Wen, L., Li, C., Chen, R., Ye, Z., Zhao, J., Pan, J. Contribution of the outer membrane protein OmpW in *Escherichia coli* to complement resistance from binding to factor H. *Microb. Pathog.* **98**, 57-62 (2016).

28. Wu, X. B., et al. Outer membrane protein OmpW of *Escherichia coli* is required for resistance to phagocytosis. *Res. Microbiol.* **164**, 848-855 (2013).

29. Gaulton, A., et al. ChEMBL: a large-scale bioactivity database for drug discovery. *Nucleic Acids Res.* **40**, D1100-D1107 (2012).

30. McKinney, W. Pandas: a foundational Python library for data analysis and statistics. Python for high performance and scientific computing, 14(9), 1-9 (2011).

31. Landrum, G. RDKit: A software suite for cheminformatics, computational chemistry, and predictive modeling. Greg Landrum, 8 (2013).

32. Probst, D., Reymond, J. L. A probabilistic molecular fingerprint for big data settings. *J. Cheminformatics* **10**, 1-12 (2018).

33. Boulaamane, Y., Jangid, K., Britel, M. R., Maurady, A. Probing the molecular mechanisms of α-synuclein inhibitors unveils promising natural candidates through machine-learning QSAR, pharmacophore modeling, and molecular dynamics simulations. *Mol. Div.* 1-17 (2023).

34. Jumper, J., et al. Highly accurate protein structure prediction with AlphaFold. *Nature* **596**, 583-589 (2021).

35. Heo, L., Park, H., Seok, C. GalaxyRefine: Protein structure refinement driven by side-chain repacking. *Nucleic Acids Res.* **41**, W384-W388 (2013).

36. Laskowski, R. A., MacArthur, M. W., Moss, D. S., Thornton, J. M. PROCHECK: a program to check the stereochemical quality of protein structures. *J. Appl. Crystallogr.* **26**, 283-291 (1993).

37. Wiederstein, M., Sippl, M. J. ProSA-web: interactive web service for the recognition of errors in three-dimensional structures of proteins. *Nucleic Acids Res.* **35**, W407-W410 (2007).

38. Jendele, L., Krivak, R., Skoda, P., Novotny, M., Hoksza, D. PrankWeb: a web server for ligand binding site prediction and visualization. *Nucleic Acids Res.* **47**, W345-W349 (2019).

39. Jakubec, D., Skoda, P., Krivak, R., Novotny, M., Hoksza, D. PrankWeb 3: accelerated ligand-binding site predictions for experimental and modelled protein structures. *Nucleic Acids Res.* **50**, W593-W597 (2022).

40. Pollastri, M. P. Overview on the Rule of Five. *Curr. Protoc. Pharmacol.* **49**, 9-12 (2010).

41. Trott, O., Olson, A. J. AutoDock Vina: improving the speed and accuracy of docking with a new scoring function, efficient optimization, and multithreading. *J. Comput. Chem.* **31**, 455-461 (2010).

42. Boulaamane, Y., Ibrahim, M. A., Britel, M. R., Maurady, A. *In silico* studies of natural product-like caffeine derivatives as potential MAO-B inhibitors/AA2AR antagonists for the treatment of Parkinson's disease. *J. Integr. Bioinform.* **19**, 20210027 (2022).

43. Huey, R., & Morris, G. M. Using AutoDock 4 with AutoDocktools: a tutorial. The Scripps Research Institute, USA, 54, 56 (2008).

44. Soojhawon, I., Pattabiraman, N., Tsang, A., Roth, A. L., Kang, E., Noble, S. M. Discovery of novel inhibitors of multidrug-resistant *Acinetobacter baumannii. Bioorg. Medicinal Chem.* **25**, 5477-5482 (2017).

45. Abraham, M. J., Murtola, T., Schulz, R., Páll, S., Smith, J. C., Hess, B., Lindahl, E. GROMACS: High performance molecular simulations through multi-level parallelism from laptops to supercomputers. *SoftwareX* **1**, 19-25 (2015).

46. Vanommeslaeghe, K., MacKerell Jr, A. D. Automation of the CHARMM General Force Field (CGenFF) I: bond perception and atom typing. *J. Chem. Inf. Model.* **52**, 3144-3154 (2012).

47. Abraham, M. J., Gready, J. E. Optimization of parameters for molecular dynamics simulation using smooth particle-mesh Ewald in GROMACS 4.5. *J. Computational Chem.* **32**, 2031-2040 (2011).

48. Boulaamane, Y., Ibrahim, M. A., Britel, M. R., Maurady, A. *In silico* studies of natural product-like caffeine derivatives as potential MAO-B inhibitors/AA2AR antagonists for the treatment of Parkinson's disease. *J. Integr. Bioinform.* **19**, 20210027 (2022).

49. Boulaamane, Y., Kandpal, P., Chandra, A., Britel, M. R., Maurady, A. Chemical library design, QSAR modeling and molecular dynamics simulations of naturally occurring coumarins as dual inhibitors of MAO-B and AChE. *J. Biomol. Struct. Dyn.* **18**, 1-18 (2023).

50. Genheden, S., Ryde, U. The MM/PBSA and MM/GBSA methods to estimate ligand-binding affinities. *Expert Opin. Drug Discov.* **10**, 449-461 (2015).

51. European Committee on Antimicrobial Susceptibility Testing. (2023). European antimicrobial breakpoints. Basel: EUCAST.

52. Miró-Canturri, A., Ayerbe-Algaba, R., Villodres, Á.R., Pachón, J., Smani, Y. Repositioning rafoxanide to treat Gram-negative bacilli infections. *J. Antimicrob. Chemother.* **75**, 1895-1905 (2020).

53. Parra-Millán, R., et al. Intracellular trafficking and persistence of *Acinetobacter baumannii* requires Transcription Factor EB. *mSphere* **3**, e00106-18 (2018).

Tables

Table 1. Performance metrics of the generated classification models on the testing and validation sets.

Dataset	Model	SE	SP	Q+	Q-	ACC	MCC
Testing set	Random Forest	0.89	0.92	0.88	0.94	0.91	0.82
	Support Vector Machine	0.88	0.91	0.85	0.93	0.90	0.78
	K-Nearest Neighbors	0.88	0.93	0.88	0.92	0.91	0.80
	Naive Bayes	0.58	0.96	0.96	0.56	0.72	0.53
	Convolutional Neural Network	0.83	0.96	0.95	0.88	0.90	0.81
Validation set	Random Forest	0.86	0.91	0.86	0.91	0.89	0.77
	Support Vector Machine	0.81	0.91	0.86	0.87	0.87	0.72
	K-Nearest Neighbors	0.79	0.96	0.94	0.85	0.88	0.77
	Naive Bayes	0.53	0.93	0.94	0.49	0.66	0.45
	Convolutional Neural Network	0.81	0.97	0.96	0.86	0.90	0.80

SE: Sensitivity (true positive rate); SP: Specificity (false positive rate); Q+: positive predictive value; Q-: negative predictive value; ACC: Accuracy; MCC: Matthews' correlation coefficient.

Table 2. Structure-based virtual screening results of the selected natural compounds against OmpW of A. baumannii.

Compound	Binding score (kcal/mol)	Hydrogen bonds	Hydrophobic interactions
Amb22174074	-7.8	GLN-23, SER-193, LYS-195	PHE-59, HIS-101, ASN-144, GLN-146, LYS-195
Amb8401505	-7.7	GLN-23, PHE-102, ASN-104, ASN-144, TRP-153, SER-193	PHE-59, HIS-101, LYS-103, ASN-144, LYS-195
Amb2698241	-7.5	GLN-23, HIS-101, SER-193, LYS-195	PHE-59, THR-109, ASN-144, GLN-146, LYS-195
Amb8399162	-7.4	GLN-23, ASN-104, SER-193, LYS-195	PHE-59, LYS-103, THR-109, ASN-144, LYS-195
Amb8401506	-7.4	PHE-102, ASN-104, GLN-146, LYS-195	PHE-59, HIS-101, LYS-103, LYS-195
Amb22172936	-7.4	GLN-23, ARG-107, THR-109, TRP-153, LYS-195	HIS-101, LYS-103, THR-109, ASN-144, GLN-146, LYS-195
Amb22173712	-7.4	GLN-23, THR-109, SER-193, LYS-195	PHE-59, HIS-101, LYS-103, THR-109, ASN-144, GLN-146, LYS-195
Amb10550080	-7.3	GLN-23, ASN-104, THR-109, ASN-152, SER-193	PHE-59, HIS-101, LYS-195
Amb23604248	-7.2	ASN-104, THR-109, ASN-144, GLN-146, SER-193	PHE-59, LYS-103, THR-109
Amb23604228	-7.0	GLN-23, ASN-104, ASN-144, SER-193, LYS-195	GLN-23, ASN-104, ASN-144, SER-193, LYS-195

Table 3. ADME properties prediction results for the selected compounds.

Compound	LogPo/w	LogS	GI absorption	BBB	P-gp substrate	PAINS
Amb22174074	4.14	-4.88	High	Yes	No	0 alert
Amb8401505	2.77	-3.73	High	No	No	Catechol_A
Amb2698241	3.00	-3.92	High	No	No	0 alert
Amb8399162	3.48	-4.01	High	Yes	No	0 alert
Amb8401506	3.16	-3.87	High	Yes	No	Catechol_A
Amb22172936	3.03	-4.17	High	Yes	No	0 alert
Amb22173712	3.55	-4.02	High	Yes	No	0 alert
Amb10550080	2.16	-3.11	High	No	No	Catechol_A
Amb23604248	2.11	-3.11	High	No	No	Catechol_A
Amb23604228	2.86	-3.39	High	Yes	No	0 alert

Table 4. List of average and standard deviations of all energetic components including the binding energy taken from MM-PBSA analysis.

Complex	MMPBSA (kJ/mol)				
	ΔG_{bind}	ΔG_{vdW}	ΔG_{elec}	ΔG_{solv}	ΔG_{sasa}
Amb22174074	-35.03±20.08	-118.74±16.41	-45.52±24.70	144.30±33.25	-15.10±1.63
Amb8401505	-41.92±17.02	-122.42±15.16	-42.96±15.32	139.20±22.25	-15.74±1.58
Amb2698241	-45.23±17.96	-115.48±18.37	-37.25±11.57	122.31±23.21	-14.81±1.54
Amb8399162	-39.11±16.56	-143.59±18.84	-35.11±16.60	156.61±30.64	-17.01±1.94

ΔG_{bind}: Binding energy; ΔG_{vdW}: van der Waals energy; ΔG_{elec}: Electrostatic energy; ΔG_{solv}: Polar solvation energy; ΔG_{sasa}: Solvent accessible surface area energy.

Table 4. MIC results for the studied compounds against different wild type, colistin-resistant and OmpW-deficient A. baumannii.

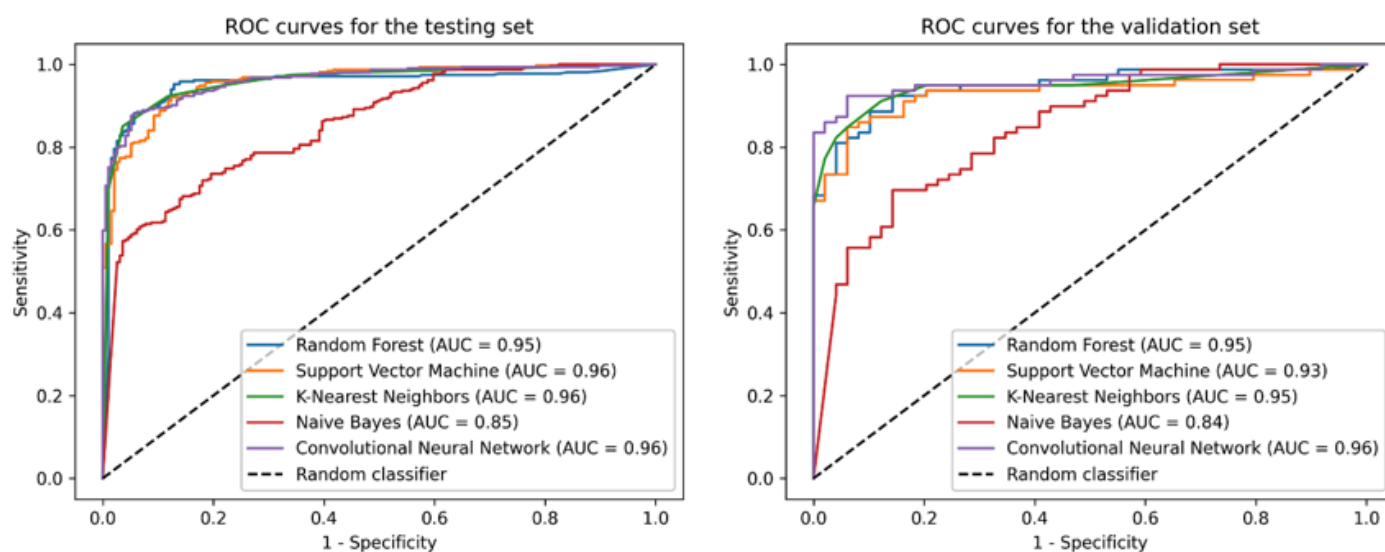| A. baumannii strain	MIC (mg/L)	
	Colistin	Demethoxycurcumin
ATCC 17978	0.25	64
ATCC17978 ΔOmpW	0.25	64
Ab11	256	64
Ab20	64	64
Ab21	128	64
Ab22	128	64
Ab99	64	64
Ab113	256	64
CR17	32	64

Figures

ROC curves for the testing set — Random Forest (AUC = 0.95), Support Vector Machine (AUC = 0.96), K-Nearest Neighbors (AUC = 0.96), Naive Bayes (AUC = 0.85), Convolutional Neural Network (AUC = 0.96), Random classifier.

ROC curves for the validation set — Random Forest (AUC = 0.95), Support Vector Machine (AUC = 0.93), K-Nearest Neighbors (AUC = 0.95), Naive Bayes (AUC = 0.84), Convolutional Neural Network (AUC = 0.96), Random classifier.

Figure 1

ROC curves and AUC values depict the performance of the generated QSAR classification models on the testing and validation sets.
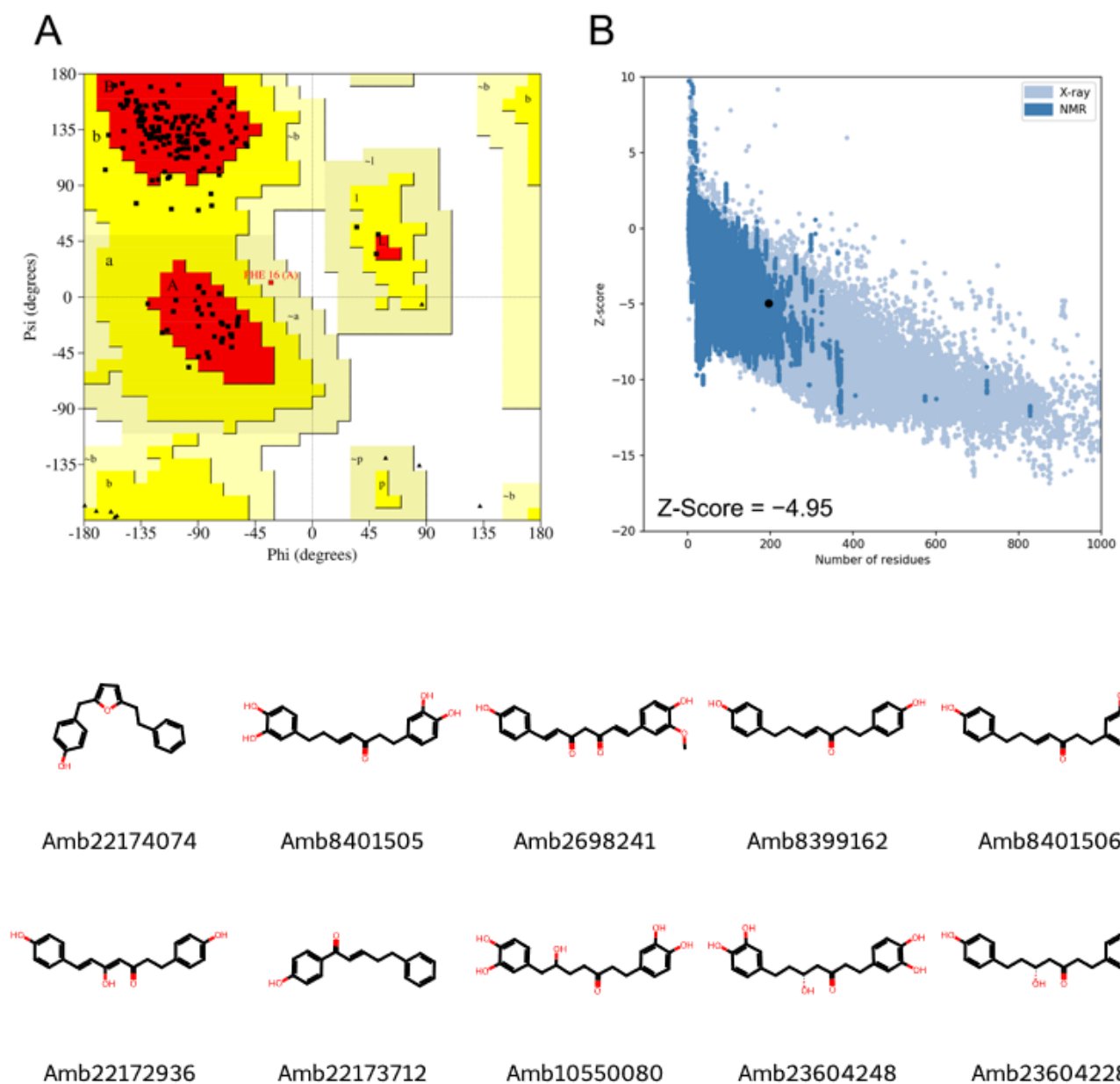
Figure 2

PROCHECK tool was used to create Ramachandran plots for OmpW (**A**). Additionally, the overall model quality for OmpW was assessed using PROSA-web, revealing a Z-Score of -4.95 (**B**). Chemical structures of the top ten highest-scoring compounds against OmpW (**C**).
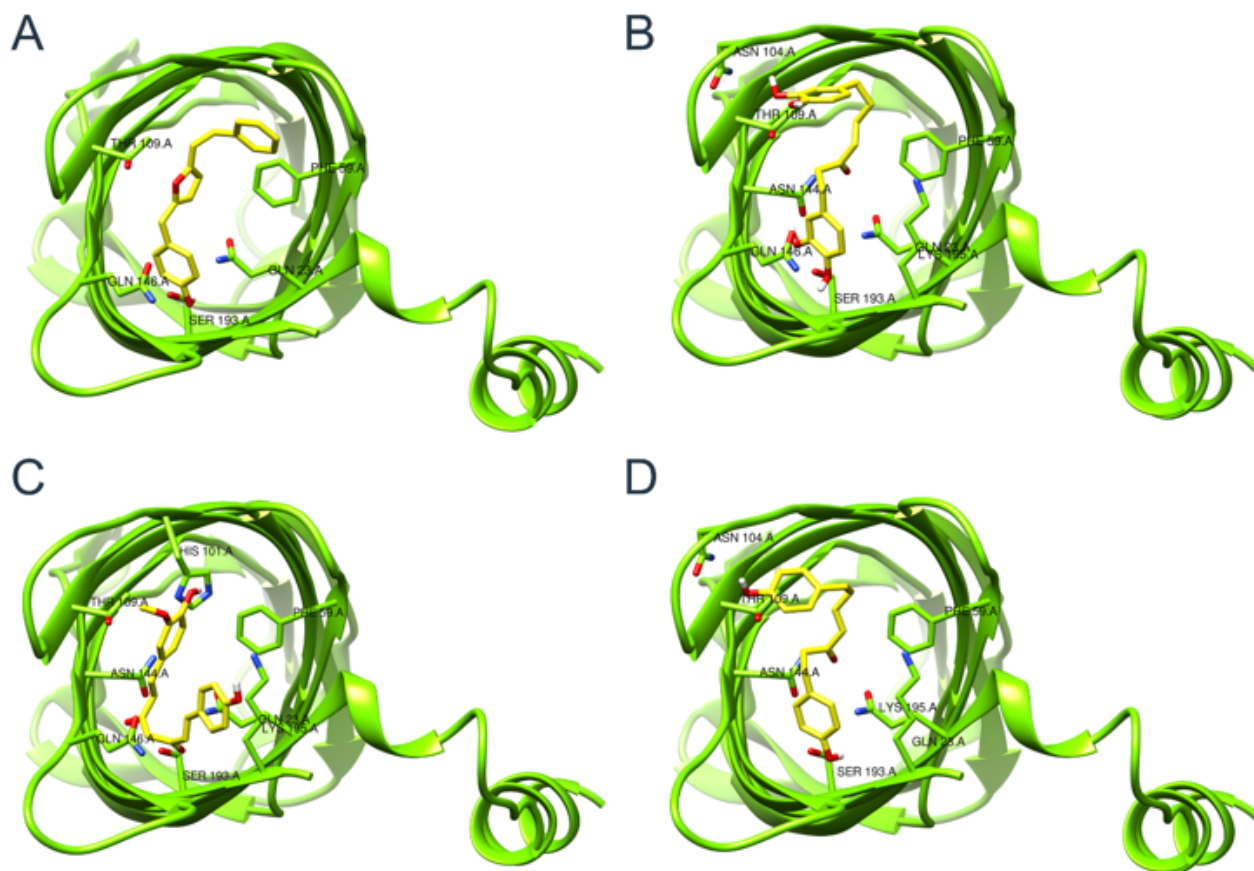
Figure 3

Binding conformations of the top four highest-ranking natural products: Amb22174074 (**A**), Amb8401505 (**B**), Amb2698241 (**C**), and Amb8399162 (**D**) in complex with OmpW's periplasmic region.
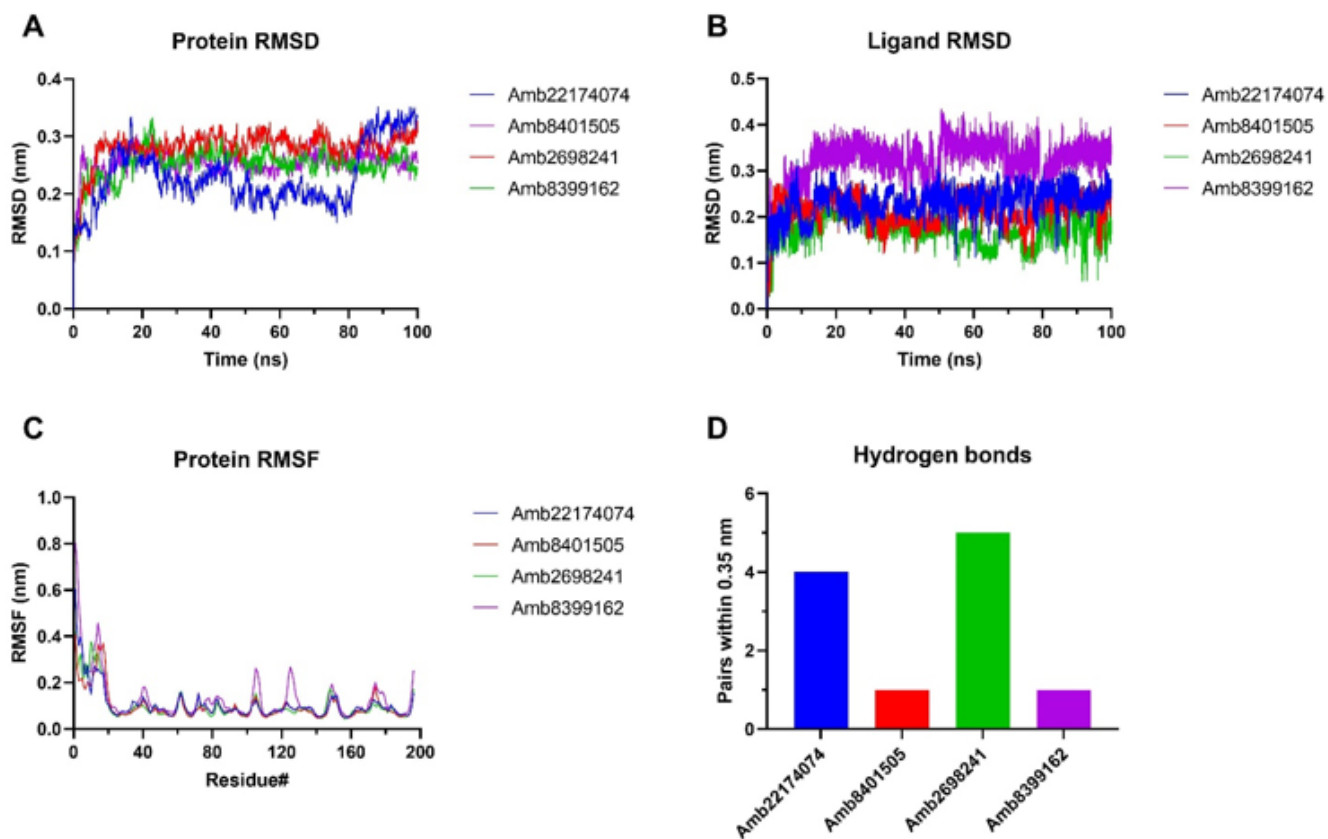
Figure 4

Molecular dynamics simulations analysis through Protein RMSD (**A**), Ligand RMSD, (**B**), RMSF (**C**) and hydrogen bonds at 100 ns (**D**).
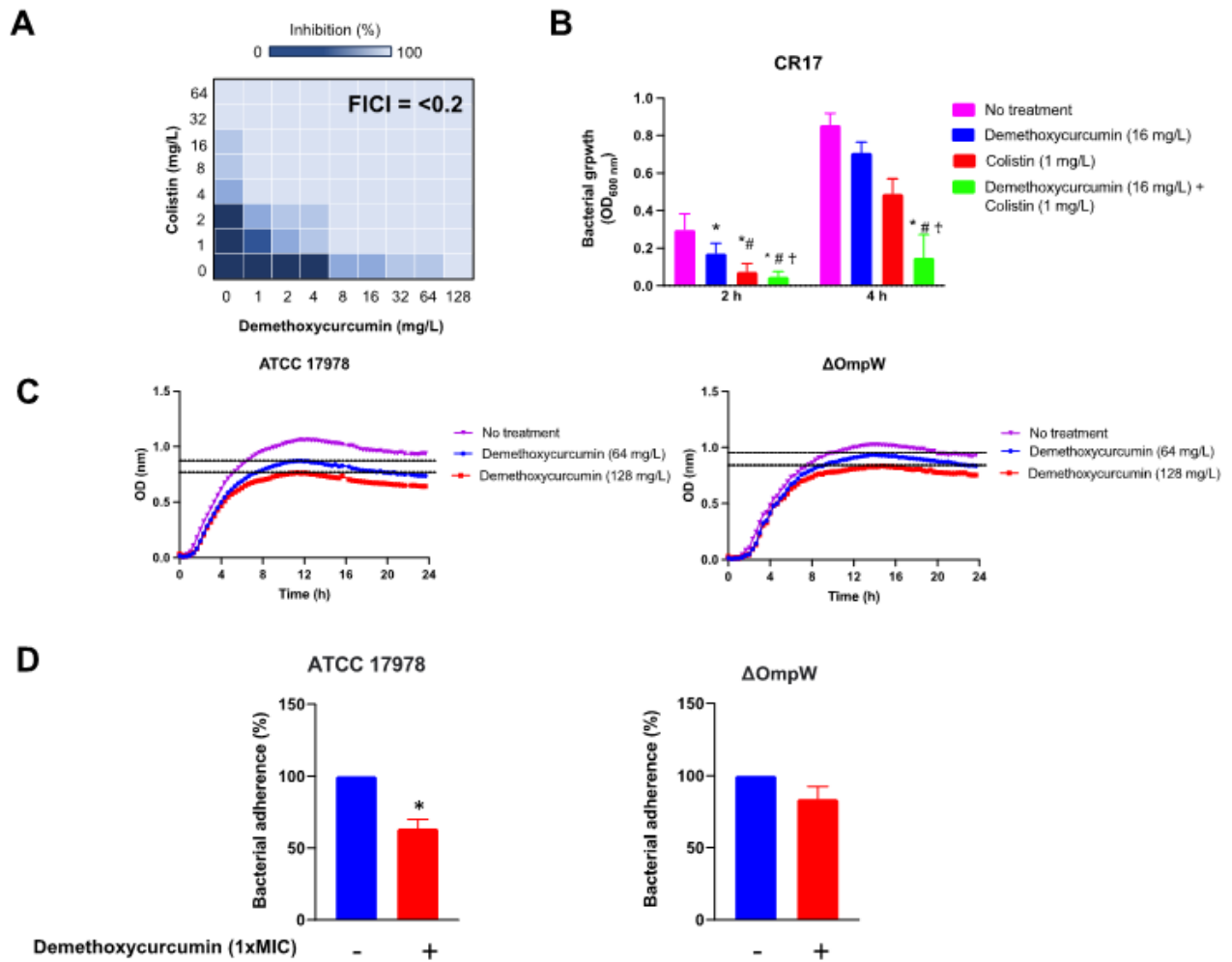
Figure 5

In vitro antibacterial activity of demethoxycurcumin. Representative heat plots of microdilution checkerboard assay for the combination of colistin and demethoxycurcumin against colistin-resistant A. baumannii CR17 strain (**A**). Bacterial growth for colistin and demethoxycurcumin monotherapy and combination therapy against colistin-resistant A. baumannii CR17 strain during 24 h incubation. The concentrations of colistin and demethoxycurcumin are 1 and 16 mg/L, respectively, *P<0.05: treatment vs no treatment, [#]P<0.05: colistin vs demethoxycurcumin, [†]P<0.05: colistin vs demethoxycurcumin plus colistin (**B**), Bacterial growth curve plots of A. baumannii ATCC 17978 and A. baumannii ΔOmpW (**C**) in the absence and presence of demethoxycurcumin treatment at different concentrations. Analysis of A. baumannii ATCC 17978 and ΔOmpW adhesion to HELA host cells with and without demethoxycurcumin treatment, *P<0.05: treatment vs no treatment (**D**).

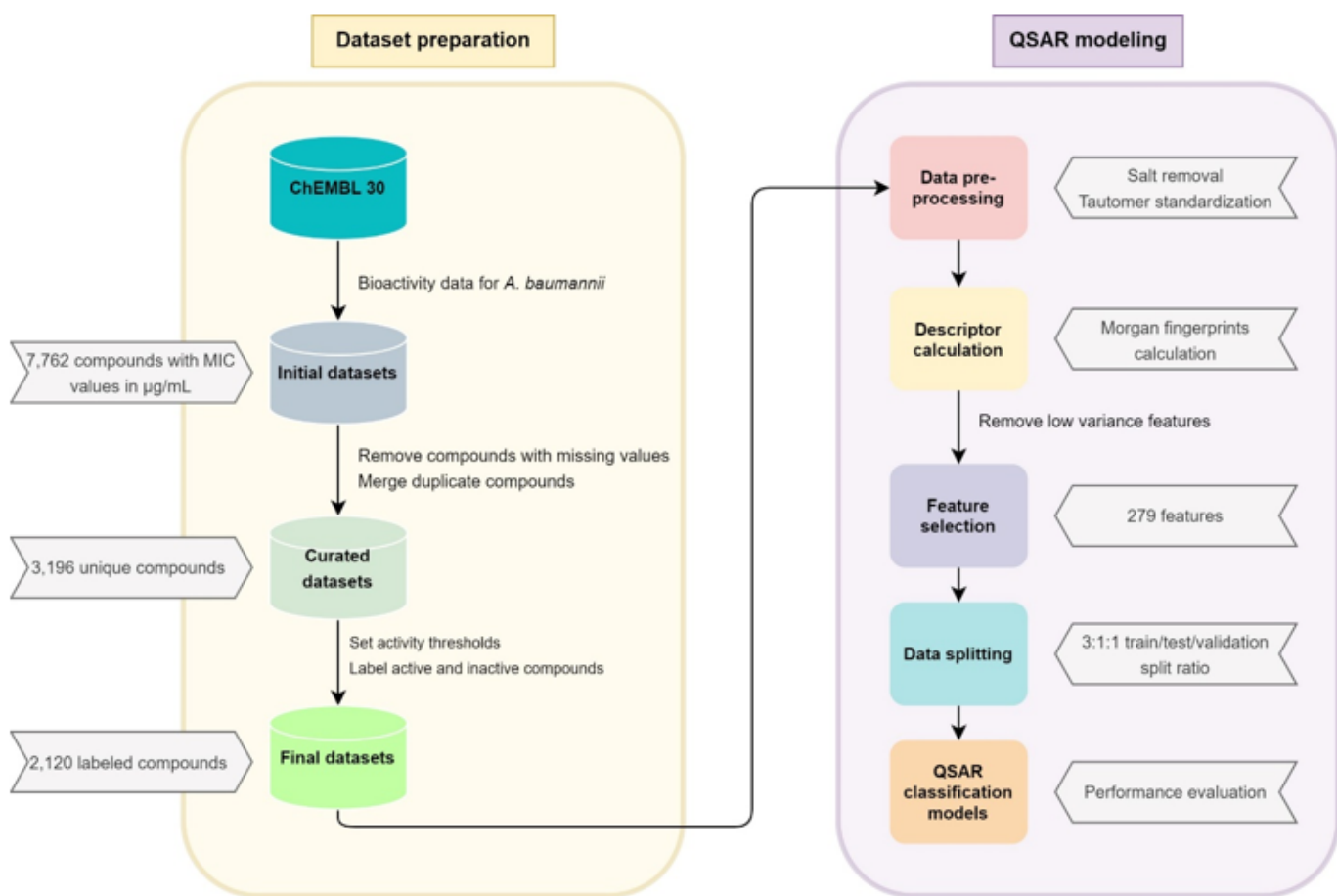**Figure 6**

QSAR modeling workflow to predict novel compounds against A. baumannii.

Supplementary Files

This is a list of supplementary files associated with this preprint. Click to download.

- SUPPLEMENTALDATA.docx